PHYSICAL REVIEW B VOLUME 45, NUMBER 11 15 MARCH 1992-I

Sapphire $(11\bar{2}0)$ surface: Structure and laser-induced desorption of aluminum

M. A. Schildbach
Department of Applied Science, University of California at Davis/Livermore, Livermore, California 94550

A. V. Hamza
Department of Chemistry and Material Science, University of California, Lawrence Livermore National Laboratory, Livermore, California 94550

(Received 27 June 1991; revised manuscript received 4 November 1991)

The laser-induced desorption of particles from a well-characterized sapphire $(11\bar{2}0)$ surface at laser wavelengths of 1064 nm (1.17 eV) and 355 nm (3.51 eV) was investigated by time-of-flight mass spectrometry. Below the laser ablation threshold, only aluminum ions were observed to desorb with average kinetic energies of 7.0 ± 0.7 eV at both photon energies. The high kinetic energies of the desorbing aluminum ions indicate that the desorption mechanism is electronic. The surface atomic and electronic structure was studied with low-energy electron diffraction (LEED), reflection electron-energy-loss spectroscopy, and Auger electron spectroscopy. After heating the surface to over 1500 K, a reconstructed surface exhbiting a (12×4) LEED pattern was established. The electron-energy-loss spectrum from the (12×4) surface revealed the presence of surface electronic states in the bulk band gap of sapphire as evidenced by a broad (~ 2 eV full width at half maximum) energy-loss feature centered at 3.6 eV. The surface electronic states are believed to participate in the photon-absorption process.

I. INTRODUCTION

In order to understand and control the processes of laser ablation and optical surface damage, the fundamental problem of identifying the initial mechanism of energy deposition in the material needs to be addressed. At long wavelengths, optical materials absorb photon energy by the creation of phonons in the material, while at short wavelengths, absorption proceeds by promotion of valence electrons to the conduction band. Between these wavelengths regimes, nominally transparent dielectric materials absorb only a small fraction of the incident light. However, as the light intensity is increased, this absorption eventually leads to laser etching of the surface. The interaction of laser radiation with optical materials is commonly thought to involve electronic states in the bulk forbidden energy gap of the dielectric material due to the surface, defects, and impurities.[1]

Surfaces of wide-band-gap materials generally absorb photon energy more readily than the bulk, as evidenced by lower damage thresholds,[2] perhaps because of the presence of surface states and a higher concentration of defect and impurity states. The investigation of the photon-surface interaction presents an opportunity, not found in studies of the bulk, to gain insight into the absorption mechanism, primarily because the absorption can be sensitively monitored by the detection of photon-induced particle emission. A number of investigations[1,3,4] have produced information about the absorption mechanism from the yield and kinetic energy of desorbing particles. These measurements are best performed below the ablation threshold so that laser-plume interactions[5,6] and gas-phase particle collisions[7,8] are eliminated. Standard surface-analysis techniques also allow the characterization of the stoichiometry and structure of the laser-irradiated surface and may be helpful in sorting out the effects of sample preparation on the photon-surface interaction. An example of the importance of surface condition is seen in the differences in emission from cleaved[9] and polished[1] BaF_2 surfaces.

Sapphire (α-Al_2O_3) was chosen for study because of its wide band gap (~ 9 eV) and the fact that, unlike the majority of insulators, it may be characterized easily using surface electron spectroscopies. Sapphire has been the subject of a number of previous experimental and theoretical investigations due to its technological importance as an electronic and optical material.

The surface atomic structure of all of the low-index planes of sapphire has been investigated by low-energy electron diffraction (LEED) (Refs. 10–13) primarily in relation to silicon-on-sapphire epitaxy. These surfaces show a rich variety of reconstructions upon annealing in vacuum to ~ 1500 K, including the $(11\bar{2}0)$ surface which was described by Chang[10] as having a complex LEED pattern. Because of the large number of unit cells involved in the reconstruction, an appropriate model for the geometric surface structure is lacking.

Only a limited number of studies of the electronic structure of sapphire surfaces has been done. The majority of the work has been concentrated on electron-energy-loss spectroscopy (ELS) of polycrystalline samples[14,15] and the $(1\bar{1}02)$ surface.[16] In all three experiments, energy-loss features with energies less than the ~ 9-eV band gap were present. Williams and co-workers,[16] using x-ray photoemission spectroscopy (XPS) data, have assigned an energy-loss feature at ~ 4.7 eV to

©1992 The American Physical Society

a transition from the valence-band maximum (VBM) to an empty surface state and have suggested that this state contributes to surface conductivity. Haynes *et al.*[17] have postulated the existence of a surface electronic state on the (0001) surface of Al_2O_3 to explain the quenching of fluorescence lifetimes of adsorbed phenanthrene.

Theoretical investigation of the electronic structure of sapphire has been stimulated by x-ray absorption measurements, x-ray photoelectron spectra, and the ELS experiments mentioned above. Several theoretical determinations of the electronic structure of Al_2O_3 analogs have been performed. Ciraci and Batra[18] have used a semiempirical method based on the extended Hückel theory to obtain results which compare favorably with existing experimental data. They have also performed calculations on thin Al_2O_3 slabs to enhance the surface contributions to the electronic structure. Their results predicted the presence of an empty surface state ~3 eV above the VBM due to the dangling bonds of the partially coordinated aluminum atoms on the (0001) surface. Dangling Al bonds are likely to be present at any bulk truncation and so such states should exist on all sapphire surfaces. Shangda *et al.*[19] have used the self-consistent local-density theory to calculate the electronic structure of a number of Al_2O_3-like clusters (e.g., $Al_{10}O_{15}$). The widths of their bands are less than those of Ciraci and Batra, but the main features are in agreement. Similarly, Evarestov *et al.*[20] using the semiempirical Mulliken-Rüdenberg method have also reproduced the main features of the electronic structure.

Laser interactions with uncharacterized sapphire surfaces have also been studied. Chase and Smith[1] were unable to detect desorption of neutral species below the ablation threshold. Laser ablation at 248 nm from the $(2\bar{1}\bar{1}0)$ surface and from oxidized Al metal was shown by Dreyfus *et al.*[5] to be electronic in nature using laser-induced fluorescence detection techniques. The high kinetic energy of the ablated aluminum (~4 eV) and AlO (~1 eV) and the relatively low rotational temperature of the AlO (600 K) ruled out a thermal process and provided support for an electronic ablation mechanism. The absorption of excimer light at 193, 248, and 351 nm by crystalline sapphire with the *c* axis on or near the surface plane was measured using pulsed photothermal deflection.[21] At laser fluences just below the ablation threshold, the fraction of energy absorbed by the surface decreased from 0.03 to 4×10^{-4} as the wavelength was increased from 193 to 351 nm. These low absorbances give rise to a maximum surface temperature of 430 K, much too low for thermal vaporization of sapphire, again pointing to an electronic mechanism. Tam and co-workers[22] observed rapid sputtering of sapphire in air at 266 nm with 3 ps pulses at high fluence (~10 J/cm^2). They hypothesize that initially the surface absorbs only weakly due to surface states, impurities, or imperfections, causing ablation of a small amount of material. The removal of material creates more imperfections, impurities, or color centers, which can absorb more light in subsequent pulses, explaining the acceleration of the laser etch rate.

This paper reports on the atomic and electronic structure of the sapphire $(11\bar{2}0)$ surface and their possible relationship to the laser-induced desorption of aluminum ions at 1064 and 355 nm. Section II is a description of the experimental apparatus and procedures. Section III (results and discussion) is divided into three parts: the atomic structure of, the electronic structure of, and laser desorption from $Al_2O_3(11\bar{2}0)$. The desorption of aluminum ions will be shown to follow an electronic mechanism.

II. EXPERIMENT

The samples were EFG (edge-defined, film-fed growth) single-crystal sapphire windows purchased from Saphikon. The manufacturer oriented the windows to the $(11\bar{2}0)$ surface (±4°) and mechanically polished them to a surface roughness of <50 nm. Typical samples were 1 mm thick and 13 mm on a side. Before mounting, the sapphire was cleaned ultrasonically in ethanol and dried with flowing argon.

All experiments were performed in a UHV chamber, shown schematically in Fig. 1, with a base pressure below 10^{-10} Torr. Following a 450 K bake of the chamber, the samples were cleaned by argon ion bombardment and annealed using temperatures of up to 1700 K. Heating of the samples was accomplished by passing up to 50 A through two 4-mm wide, 0.03-mm thick tantalum strips sandwiched between two sapphire windows as described by Gignac, Williams, and Kowalczyk.[16] Placing the strips at the top and bottom of the windows provided a clear aperture through which the laser beam could pass. Temperatures were measured with a Chromel-Alumel (*K*-type) thermocouple attached to the surface with a high-temperature ceramic adhesive.[17] Heating and cool-

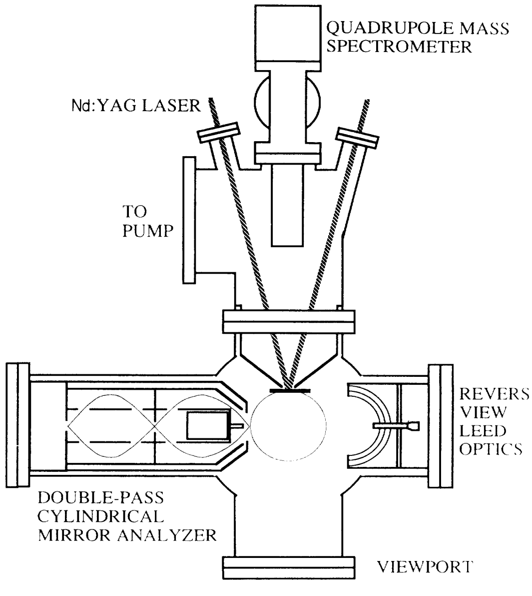

FIG. 1. Chamber schematic. Nd:YAG laser light at the fundamental and third harmonic are incident at 15° from the surface normal. The quadrupole mass spectrometer is in line of sight of the sample and differentially cryopumped. The aperture between the main and differential pumping is 6.4 mm.

ing were computer controlled and rates of 1.0 and -0.3 K/s, respectively, were used during cycles to minimize thermal stress cracking and so retain a good optical surface.

Surface structure and composition were monitored with standard electron spectroscopies. The surface atomic structure was examined using reverse-view LEED optics (Princeton Research Instruments). A PHI 15-255 GAR double-pass cylindrical mirror analyzer with a coaxial electron gun was used to collect Auger electron and reflection electron-energy-loss spectra. Auger data were taken using lock-in detection with a 3-eV peak-to-peak modulation, 3-keV incident electron beam energy, and a beam current of 1–5 μA. For the energy-loss measurements pulse counting was used with an incident energy of 200 eV, a current <200 nA, and a pass energy of 50 eV. The resolution was defined by the 0.8-eV full width half maximum energy spread of the incident electron beam. Typical EL spectra took 15 min to collect. During the collection of both types of spectra, the electron beam was incident normal to the sample surface.

A Nd:YAG (Lumonics JK HY750) laser was used to expose surfaces to either the fundamental wavelength of 1064 nm with a pulse width of 8 ns or the third harmonic at 355 nm with a pulse width of 6 ns. The beam energy was controlled using a half-wave plate and a thin-film polarizer and was monitored by directing the reflection from a fused silica flat into a surface pyroelectric joule meter. Using a 50-cm focal length fused silica lens, the beam was focused down to a $1/e^2$ radius of 0.5 mm, as determined by knife edge profiling. The laser light was incident 15° from the sapphire surface normal.

Laser-desorbed particles were detected with a Balzers QMA 400 quadrupole mass analyzer with a cross-beam ion source and a 90° off axis electron multiplier. Having the multiplier off axis prevents production of signals by photons or neutral particles, which are not affected by the mass filter. However, the 90° cylindrical plates used to deflect the filtered ions onto the first dynode of the electron multiplier also act as an energy filter, which may produce errors in the collection of time-of-flight spectra. Since the absolute energy resolution of such analyzers decreases as the pass energy is increased,[23] ions exiting the mass filter were accelerated by a 450-V potential on the outer deflection plate before being deflected. The potential difference between the two plates was accordingly set for a pass energy of 450 eV. An ion gun aimed down the axis of the quadrupole was used to measure the energy discrimination of this arrangement and it was found that the full width at 80% of maximum was ~80 eV. Further tests involving the time of flight of ions produced by laser irradiation of stainless steel showed that the spectra were unchanged with accelerating voltages producing ion energies from 390 to 510 eV. The time-of-flight distribution of ions accelerated to even 700 eV appeared unchanged, although the signal was sharply attenuated.

When used to detect neutral particles, the quadrupole, with the exception of the deflection plates and electron multiplier voltages, was set up as for residual-gas analysis. Transit time through the mass analyzer for particles initially having thermal velocities was determined by measuring the delay between a modulation of the filament potential, which turned the ionizer on and off, and modulation of the quadrupole signal. When detecting positive or negative ions, all potentials on the mass analyzer, except for those on the rods, deflector and electron multiplier, were set to ground to provide a drift tube.

The differentially pumped quadrupole was mounted such that the axis of the mass filter was along the sample surface normal. The ionizer was 220 mm from the sample, resulting in a 460-mm flight distance to the deflection plates. Signals from the electron multiplier of the mass analyzer were sent through a capacitive coupler, since the output of the electron multiplier was usually above ground potential, into an amplifier and then to a Nicolet 370 signal averager with a time resolution of 1 μs per channel. The Nicolet signal averager was triggered using the amplified signal of a photodiode located behind a turning mirror. This system permitted the observation of individual ion peaks on the signal averager.

A 17-stage Cu-Be electron multiplier mounted at 15° from the surface normal was used in parallel with the quadrupole for charged particle detection. The first dynode was 475 mm from the sample surface and the signal was capacitively coupled out, put through an amplifier, and sent to the second channel of the Nicolet signal averager.

III. RESULTS AND DISCUSSION

A. Surface atomic structure

After chamber bakeout, Auger electron spectroscopy (AES) showed the surface to be contaminated with carbon, and no LEED pattern was observed. Heating the sample to 700 K, after ion sputtering to remove the carbon, produced a (1×1) pattern, and subsequent annealing to 900 K resulted in a (3×1) structure. Annealing to surface temperatures above 1500 K produced a (12×4) reconstruction (Fig. 2), which was stable to temperatures of 1700 K. If the sample was heated without first sputtering, no pattern was visible for annealing temperatures below 1100 K and a clear (12×4) pattern was seen after heating to 1500 K. The carbon contamination apparently inhibited reconstruction of the surface and was not removed until the surface was heated to over 1100 K.

The observed (12×4) equilibrium pattern is different from, though similar to, that reported by Chang.[10] Chang described the equilibrium pattern he observed as a superposition of two Bravais lattices, neither of which was simply related to the (1×1) bulk truncation geometry. This difference may have its origins in the heating cycles used. Chang heated his samples to their final temperature in at most 30 s, while in the present work heating and cooling normally required 90 min. It is unlikely that the temperature for the equilibrium pattern was not reached in the present study since it was previously reported that sharp patterns were observable after heating to 1700 K. Additionally, the temperatures quoted by Chang were optical pyrometer measurements of the resistive tantalum heater, a method which was found in

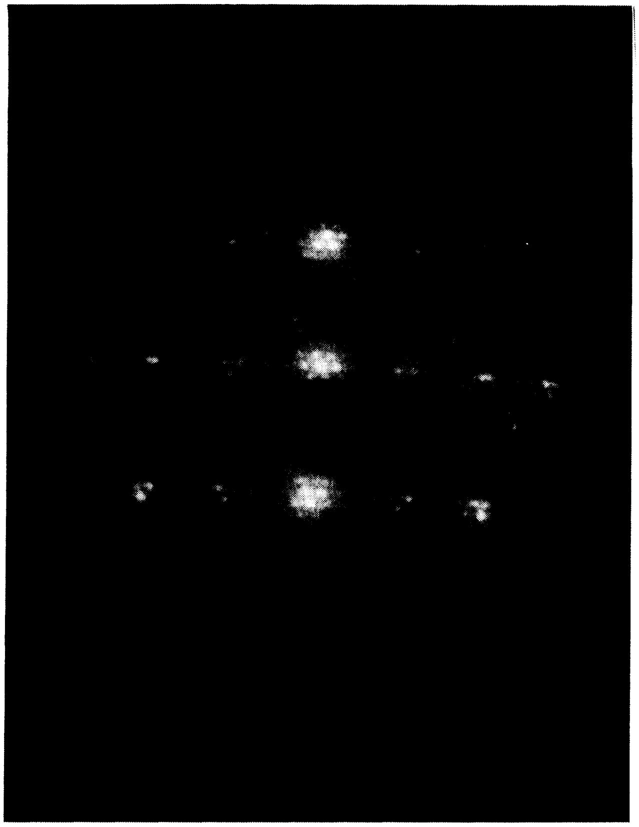

FIG. 2. Low-energy electron diffraction pattern from $Al_2O_3(11\bar{2}0)$ annealed to 1600 K. The incident beam was 5° off normal and had an energy of 143 eV.

the present work to produce temperatures ~300 K above those measured by the thermocouple attached to the sample surface.

Another possible explanation for the difference in the observed equilibrium patterns may be the precision of the sample orientation. A typical sample on which the (12×4) reconstruction was observed was found to be oriented within 1° using x-ray (Laue) diffraction. Two of the samples supplied by Saphikon did not produce the (12×4) pattern, but something quite similar to it with more diffraction beams. This was determined to be the result of a spot splitting along the $\langle 1\bar{1}00\rangle$ direction. This suggests that the complex overlayer observed by Chang may have been the result of a slightly misaligned crystal.

The (12×4) reconstruction was very stable, showing little degradation even after 10 days at 10^{-10} Torr. The surface was also stoichiometric[24] as determined by Auger electron spectroscopy, and no changes were observed in the Al to O peak-height ratio on going from the (1×1) to the (12×4). It was possible to remove the reconstruction by ion bombardment, but without altering the Al to O peak-height ratio. The secondary electron emission crossover, the incident electron energy where secondary electron emission compensates for electron capture, was ~70 eV for the (12×4) surface. Thus, at 70 eV and below, the surface charges sufficiently that LEED patterns are unstable.

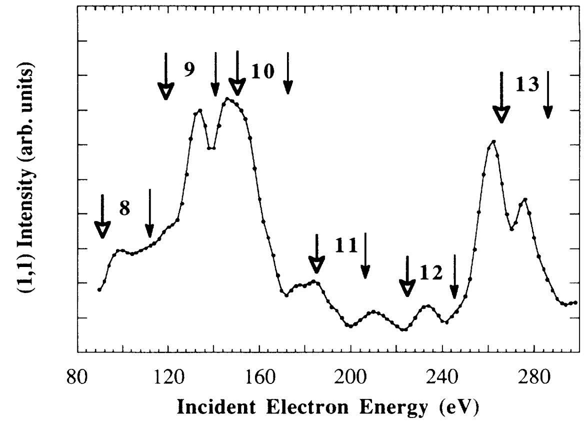

FIG. 3. LEED *I-V* curve for the (1,1) diffraction beam for the $Al_2O_3(11\bar{2}0)$-(12×4) surface. The calculated positions of the Bragg diffraction peaks are shown (small arrows), as are the Bragg peaks corrected by the 22-eV inner potential proposed by Wei and Smith (Ref. 13) (large arrows). The order of the peaks is given by the number between each pair of arrows.

An intensity versus voltage curve for the (1,1) spot of the (12×4) surface using electrons incident along the surface normal is shown in Fig. 3. Patterns for the various incident electron energies were first recorded on video tape. These images were then digitized and the spot intensity referenced to the background was determined. Shown also are the calculated Bragg energies[25,26] for an interlayer spacing of 4.76 Å, the unit-cell repeat distance, and these energies corrected with the 22-eV crystal or inner potential suggested by Wei and Smith[13] (Fig. 3). The value of the crystal potential seems appropriate, but kinematic theory does not adequately describe the scattering process in this case. The observed peak extinctions are not accounted for by the structure factor and the splitting of the $n = 10$ and 13 peaks cannot be predicted by this simple model.

Surface composition and electron effects on the surface were determined by AES. An Auger electron spectrum

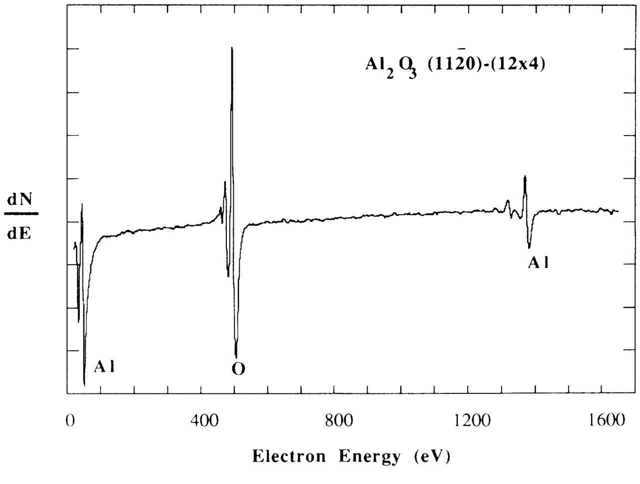

FIG. 4. Auger electron spectrum for the $Al_2O_3(11\bar{2}0)$-(12×4) surface.

of the (12×4) surface is shown in Fig. 4. The two peaks at 34 and 52 eV are due to Al (*LVV*) transitions and the 506-eV peak is from O (*KVV*) electrons. The group of peaks around 1350 eV is from Al (*KLL*) processes After large electron exposures a third Al peak appeared at 63 eV, indicating the presence of metallic aluminum.[27] The appearance of this peak is attributed to oxygen desorption and subsequent formation of Al-Al bonds.

The potential for producing defects by electron bombardment with which laser light could readily interact, as seen in sodium trisilicate glass,[28] prompted an effort to determine if the electron beam damage could be repaired by annealing. The 63-eV peak could be removed by heating to 1300 K, implying an activation energy of 3.5 eV (340 kJ/mol) for the defect removal process assuming first-order kinetics and a preexponential factor of 10^{13} s^{-1}. Consequently, after characterization the surface temperature was taken to 1300 K before laser exposure.

B. Surface electronic structure

The electronic structure of the (11$\bar{2}$0)-(12×4) surface was investigated using ELS. A typical spectrum is shown in Fig. 5. The lower curve was collected using a primary current of 10 nA; the upper curve, a scan over the band-gap region, used a 150-nA current to lower the signal-to-noise ratio. For purposes of comparison with previous work, the numerically doubly differentiated spectrum is presented in Fig. 6. The most prominent feature in both spectra is due to the bulk plasmon which has an energy of 22 eV, in agreement with previous measurements.[13,14,16] Two lower-energy peaks at 13.5 and 10.4 eV are also visible in the differentiated spectrum, these being due to transitions to the conduction band.[16] Most interesting, however, is the presence of an energy-loss peak within the band gap having a value of 3.6 eV in Fig. 5 and 4.3 eV in Fig. 6. The difference in the energies of the two peaks is within the resolution (0.8 eV) of the measurement, but the superior signal-to-noise ratio suggests that the 3.6-eV peak energy is more accurate. The breadth of the peak, 2 eV FWHM (where FWHM denotes full width at half maximum), indicates that more than one surface electronic state may be present in the band gap.

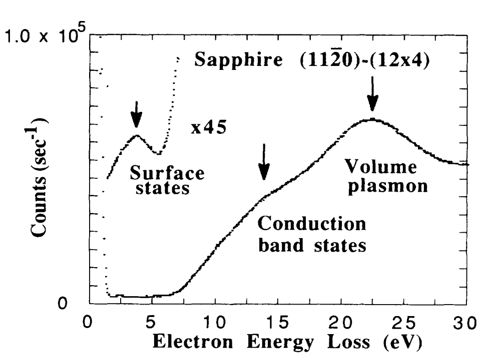

FIG. 5. The reflection electron-energy-loss spectrum for Al_2O_3(11$\bar{2}$0)-(12×4). The primary electron energy is 200 eV. The elastic peak had 1.6 million counts per second and a full width at half maximum of 0.8 eV. The inset portion is a higher sensitivity scan of the band-gap region.

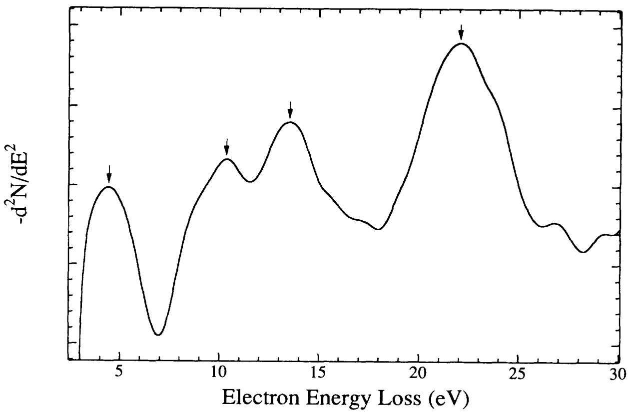

FIG. 6. Doubly differentiated reflection electron-energy-loss spectrum for Al_2O_3(11$\bar{2}$0)-(12×4). The spectrum is a numerical double differentiation of the spectrum shown in Fig. 5.

These spectra are similar to those of Gignac, Williams, and Kowalczyk[16] for the (1$\bar{1}$02) surface and Balzarotti *et al.*[15] for self-supported polycrystalline films, both of which have a prominent energy-loss feature at ~5 eV. The energy-loss spectrum presented by Olivier and Poirier[14] for pyrolitic polycrystalline films is also quite similar, but lacks any sizable low-energy-loss features. The presence of three minute peaks at 3.8, 4.2, and 5 eV is ascribed to the creation of suboxides by electron-beam desorption of oxygen and is compared to results from the early oxidation of silicon. Studies of Al,[29,30] however, show that low oxygen coverages allow a 7-eV single electron excitation from the O (2*p*) level to the Al conduction band. It has been suggested[16] that the low-energy-loss features observed by Olivier and Poirier[14] are due to sample growth conditions.

The contention of Olivier and Poirier that Al_2O_3 is susceptible to electron beam damage has been substantiated a number of times. Balzarotti and co-workers documented the appearance of aluminum plasmon loss peaks with increasing exposure to 300-eV electrons. The Auger spectrum presented by Gignac, Williams, and Kowalczyk[16] (GWK) shows signs of oxygen desorption, there being a well-developed elemental Al peak at 67 eV. If, as implied, the energy-loss data of GWK were collected on areas producing such Auger spectra, they are most likely representative of a damaged surface. The argument presented that the surface was not modified because the spectrum did not change on subsequent scans is not entirely convincing, the saturation of such effects having been documented.[27,31]

The 4.7-eV energy-loss feature reported by GWK may be entirely electron-beam induced. During the reduction measurements of Balzarotti *et al.*[15] the low-energy-loss peak does not change much. This behavior, as pointed out by GWK, is consistent with energy levels due to dangling Al bonds. Dangling Al bonds are also proposed to be the origin of surface states, so it remains to differentiate between beam-induced desorption and intrinsic surface states.

By monitoring the growth of the metallic Al Auger peak it has been determined[14,27] that an electron dose of less than 10^{20} e/cm^2 will not noticeably degrade an alumina surface. The exposure of the lower curve in Fig. 5 was $<10^{17}$ e/cm^2 and that of the upper was $<10^{18}$ e/cm^2. Thus, electron beam damage of the variety postulated by Olivier and Poirier[14] seems unlikely in this experiment, and so the 3.6-eV energy-loss peak is assigned to transitions involving intrinsic surface states.

C. Laser desorption

Laser-induced desorption of particles from the sapphire $(11\bar{2}0)$-(12×4) surface was detected with the quadrupole mass analyzer. Species monitored include H ($m/e=1$), H_2 ($m/e=2$), C ($m/e=12$), O ($m/e=16$), OH ($m/e=17$), H_2O ($m/e=18$), Al ($m/e=27$), CO ($m/e=28$), O_2 ($m/e=32$), AlO ($m/e=43$), CO_2 ($m/e=44$), Al_2 ($m/e=54$), AlO_2 ($m/e=59$), and Al_2O_3 ($m/e=102$) as neutral particles, positive ions, and negative ions. Above the ablation threshold, aluminum and oxygen neutral particles and combination thereof were laser desorbed in agreement with previous measurements.[5] Only Al^+ was detected below the ablation threshold. Background counts and the low ionization efficiency of fast moving particles may have hindered neutral detection, but no neutral particles were unambiguously detected even when hundreds of Al ions were observed.

The presence of a small number of desorbing neutral atoms could not be ruled out. At fluences which induced the desorption of a large number of ions, a signal much like the ion signal was seen with the quadrupole set up for neutral detection. Turning off the filament had little effect on the magnitude of the $m/e=27$ output, demonstrating that ions were able to pass the 40 V ion reference potential. Discrimination between ions and neutral atoms in this case by turning off the ionizing filament and comparing signal intensities was made difficult by the shot-to-shot variation in the ion yield. However, the majority of the particles seen while trying to detect neutral atoms were ions. Chase and Smith[1] were unable to detect any neutral species desorbing from an uncharacterized sapphire surface below the ablation threshold, in agreement with the present measurements.

Figure 7 shows time-of-flight spectra of aluminum ions produced by laser exposure at wavelengths of 355 and 1064 nm. It should be emphasized that the laser fluences used were well below the surface ablation thresholds, which were determined to be ~ 12 J/cm^2 for 1064 nm and ~ 3 J/cm^2 for 355 nm, in good agreement with previous measurements for laser pulse lengths of ~ 10 ns.[21,32] The Al ions were desorbed with average kinetic energies of about 7 eV, although average energies as high as 7.7 eV and as low as 6.6 eV were seen occasionally. The upper curve is a sum of spectra obtained for a fluence range of 5–8.5 J/cm^2 at 1064 nm, while the lower curve is a sum for 2.5 J/cm^2 at 355 nm The measured time-of-flight distribution, $f(t)$, has been fit with a Maxwell-Boltzmann distribution modified with a stream velocity term:

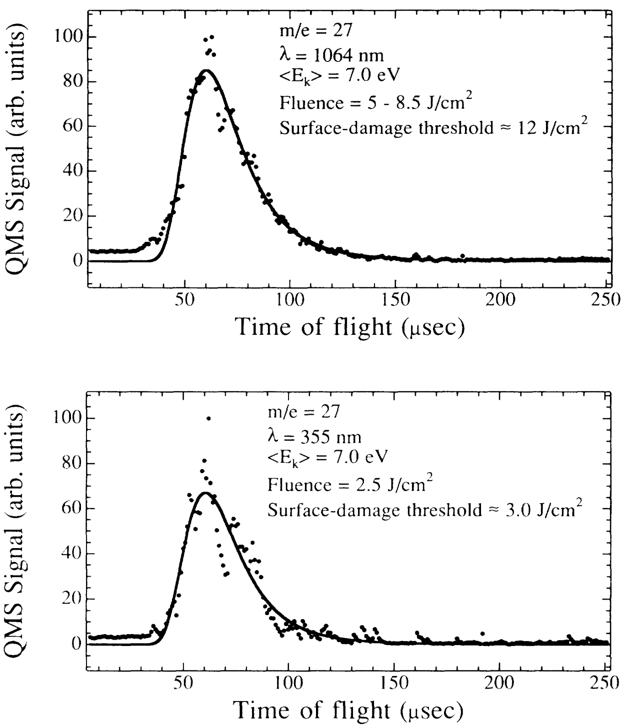

FIG. 7. Time-of-flight spectra for aluminum ions laser desorbed from $Al_2O_3(11\bar{2}0)$. Top panel shows the distribution for 1064-nm laser light; bottom panel shows the distribution for 355-nm laser light. The average kinetic energy $\langle E_k \rangle$ of the distributions is 7.0 eV for both laser wavelengths. The filled circles represent the measured ion flux; the solid line represents the modified Maxwell-Boltzmann fit to the data (see text).

$$f(t)=A_0 t^{-5}\exp\left\{-A_1\left[\left(\frac{s}{t}\right)-A_2\right]^2\right\}. \tag{1}$$

Here t is the flight time, s is the flight distance, A_0 is a normalization constant, A_1 is a measure of the width of the distribution, and A_2 is the stream velocity. If the stream velocity is zero and $A_1=m/2kT$, where m is the mass of the particle and k is Boltzmann's constant, the distribution would be a Maxwell-Boltzmann distribution at temperature T. A flux distribution is used since the ion signal is proportional to the desorbing flux and not the density, as is the case for neutral particles.[8] The offset at the beginning of the curves is caused by Q-switch noise from the laser.

Quantities such as average kinetic energy, average velocity, and average variance were calculated from velocity-weighted moments of the fitted distribution. For a flux sensitive measurement the zeroth moment of the distribution is the number of particles, whereas for a density-sensitive measurement, the first moment is the number of particles. Thus, for example, the average velocity for a flux distribution is the ratio of the first to zeroth moments, and for a density distribution the average velocity is the ratio of the second to the first moments.

Al^+ emission was observed over a wide fluence range, down to an order of magnitude below the damage (ablation) thresholds, but no well-defined emission threshold was found. Unfortunately, accurate determination of the yield as a function of laser fluence was not possible due to the small number of desorbing ions at low fluence, there normally being fewer than five ions detected per laser pulse. This may be due in part to the small solid angle seen by the electron multiplier in the mass analyzer, estimated to be 1.3×10^{-4} sr. Some compensation for the small solid angle was provided by the emission itself, which appeared to be peaked strongly along the surface normal. The ion signal at the 15° off-axis electron multiplier increased substantially when the ionizer of the quadrupole was biased positively, deflecting the Al^+ away from the quadrupole axis.

Attempts at measuring yield as a function of fluence were also hampered because only a limited number of aluminum ions could be laser desorbed. This was most obvious for laser fluences near the ablation threshold, where fairly large numbers of ions were emitted during the first two or three laser pulses, after which the yield dropped to 0–5 ions/pulse. Similar behavior is seen with lower fluences, but the decline in signal is not so well defined.

The absence of any changes in Auger and electron-energy-loss spectra upon laser exposure reinforced the conclusion that the paucity of signal reflects the paucity of desorbing particles. Some surface modification was detectable using LEED, most notably a gradual increase of the secondary-electron emission crossover with laser exposure of the surface. It has been suggested[16] that a surface electronic band is responsible for the resistance of clean sapphire surfaces to charging. The exposure of the surface to photons may disrupt this band through the desorption of aluminum, producing a shift in the crossover point.

Visible differences in the (12×4) LEED pattern other than the changes in the crossover point, such as those seen on GaP (Ref. 33) and ZnO,[34] were more difficult to produce. After 5000 pulses at 90% of the damage threshold an enlargement of LEED spots was observed. Most of the $\frac{1}{12}$th-order spots were removed after 50 000 pulses at 1064 nm at a fluence of ~3.5 J/cm^2. This is a tedious experiment since the small laser spot, 0.5 mm in diameter, has to be rastered over a sufficient area to ensure that the LEED electron beam diffracted from a laser irradiated portion of the surface. The original (12×4) pattern was restored by annealing the surface to 1500 K.

The number of desorbing ions observed per pulse and the number of pulses required to remove the fractional-order beams are in fair agreement. A (12×4) pattern implies order over 48 (1×1) cells with a total area of ~2000 Å^2. To remove completely the fractional spots, a minimum of one atom must be desorbed from each (12×4) cell. The laser beam encompassed about 10^{10} such cells, implying that an equal number of atoms need to be removed to make the reconstruction disappear. Assuming a $\cos\theta$ angular distribution (where θ is the polar angle), the geometry of the experiment would permit 40 000 atoms to be detected, or about 8 atoms/pulse for 50 000 laser pulses. Losses because of stray fields, the ion optics, and the mass filter would certainly reduce this figure, making the number of ions observed quite reasonable.

The average kinetic energy of the desorbed ions is very large, having a value near the magnitude of the band gap. Distortion of the energy distribution of desorbed particles by space-charge effects or gas-phase collisions can be ruled out due to the small number of particles desorbed and the fact that the average energy is independent of the number of ions produced per laser pulse. The kinetic energy of the aluminum ions is then directly related to the nature of the desorption, which may be modeled as a two-step process: photon absorption, followed by conversion of the acquired energy into particle momentum. Three observations suggest a plausible mechanism for the laser-induced desorption. First is the high kinetic energy (~7 eV) of the desorbing Al^+ ions; second is the observation that only aluminum is desorbed below the ablation threshold; and third is the shot-to-shot regularity of the kinetic energy of the aluminum ions.

Considering first the absorption process, the high desorption (kinetic) energy and the lack of any correlation between energy and laser fluence suggests an electronic mechanism, rather than a thermally driven process. The shot-to-shot stability of the desorption energy also suggest that the ions are not produced by fractoemission,[35] as observed by Chase and Smith[1] for NaF, since no two fractures are identical. Such a fractoemission process would be expected to yield widely varying kinetic-energy distributions (see Schildbach, Chase, and Hamza[36]).

The observation of identical distributions for both 1064- and 355-nm light suggests that both wavelengths produce the same electronic excitation involved in desorption. The unaided absorption of six 1.17-eV photons to produce surface electronic excitation capable of supplying the observed ~7 eV seems unlikely. However, the order of the photon-absorption process may be reduced by the presence of band-gap states, such as seen in the EL spectrum. From ELS it cannot be determined whether the states are filled or empty. If the states are filled, the photon absorption could be a linear process in the case of 355-nm light where the 3.51-eV photon energy matches the 3.6-eV energy-loss feature in the ELS. Similarly, the absorption of the 1064-nm light could be a low-order process if the observed surface states are filled. The reduction in the ablation threshold fluence with photon energy may be related to the lower order of the absorption at the third harmonic as opposed to the fundamental. If the surface electronic states are empty as suggested by both theory[18] and photoelectron spectroscopy,[16] they may act resonantly to enhance the valence-band excitation.[9] Wurz *et al.*[37] have reported electron stimulated emission of Li from LiF(100) at electron energies below the bulk excitation threshold. They have attributed this to excitations involving surface states.

The preferential desorption of Al ions provides an important clue to the absorption and desorption mechanisms. In more traditional photon- (Ref. 38) and electron-stimulated desorption experiments[39] on aluminum oxide where core excitations are possible only O^+ is observed to desorb. After exposure to 3-keV electrons, O^+ desorption is evidenced by the appearance of Al islands in the Auger spectra as discussed earlier. The loss of oxygen is attributed to three-hole localization on the anion following a core-level ionization and subsequent Auger decay.[40] The ionized oxygen is expelled by Coulomb repulsion. This mechanism cannot account for the desorption of Al after exposure of the surface to low-energy photons, and so it remains to address how valence excitation may produce particle desorption.

Valence excitations have produced surface sputtering in GaP (Ref. 33) and ZnO (Ref. 41) of both constituent atoms. Itoh and co-workers[33,42] have attributed this to two-hole localization brought about by the creation of a dense electron-hole plasma. Further, they have observed a Ga^+ signal,[42] which is thought to be due to the presence of Ga adatoms, that decays with laser exposure, much like the Al^+ signal seen here. In the case of covalent oxides such as SiO_2 and Al_2O_3, Itoh[34] has suggested that laser-induced sputtering would proceed by two-hole localization or reexcitation of a self-trapped exciton. In SiO_2 the excitonic mechanism is expected to result in *oxygen* desorption; the self-trapped exciton is localized on an interstial oxygen and its associated vacancy. There is no strong evidence for self-trapping of excitons in sapphire, but defects, such as aluminum adatoms, may act as traps.[34] In addition, sapphire exhibits an exciton that is centered on the aluminum[14,15] and is bound by approximately 1 eV.[43,44] Since the band gap of sapphire is ~9 eV, the exciton lies ~8 eV above the VBM. No oxygen-centered excitons have been observed for sapphire.[14,15] Thus, an exciton-mediated process could lead to the observed preferential desorption of aluminum.

The translation of the absorbed electronic energy into the observed kinetic energy of the desorbing particle must also be addressed. Such a process is generically described by the Menzel-Gomer-Redhead (MGR) mechanism,[45,46] shown schematically in Fig. 8. The lower curve represents the ground-state aluminum-surface potential interaction as a function of the aluminum-surface separation. The upper curve represents the excited state aluminum-surface potential interaction that the system can access. In this model photons are first absorbed, producing an excitation at or near the surface. Once this excitation is localized on or near a surface Al atom, it causes a transition for the Al-surface interaction to an excited-state repulsive potential resulting in desorption. The fact that ions are desorbed could be intrinsic to the excited-state potential that the laser excitation accesses. Alternatively, the ions could be the result of gas-phase ionization of neutral aluminum by photons or photoelectrons; though photoionization seems unlikely due to the fact that the ion yield was not significantly different for similar fluences of infrared and blue light. According to the model, the observed kinetic energy of the desorbing aluminum particle depends on the relaxation of the surface. If the surface remains in an excited state, only a portion of the excitation energy will appear as kinetic energy. If, on the other hand, the surface relaxes during the desorption event to its ground state, the particle will desorb with a substantial fraction of the initial excitation energy. In this case a single hole or exciton could have enough excitation energy to produce the measured kinetic energy.

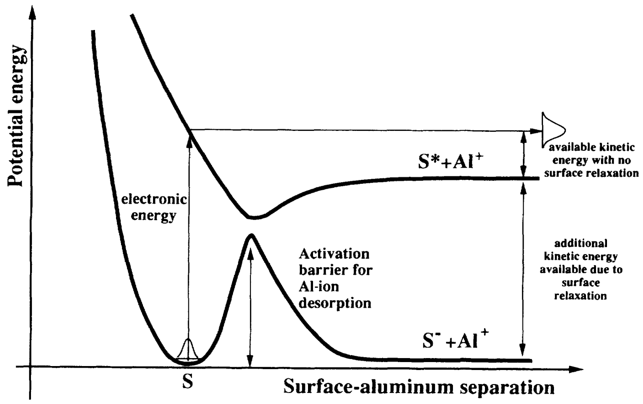

FIG. 8. Schematic representation of a possible desorption induced by electronic transitions (DIET) mechanism for Al ions from sapphire (11$\bar{2}$0). Shown are potential-energy curves for the aluminum-sapphire surface interaction. The lower curve is the ground-state potential energy as a function of aluminum atom-surface separation. The upper curve is the excited state aluminum-surface potential. The observed kinetic energy depends on the surface relaxation during the desorption event. Drawn are two limiting cases for the observed kinetic energy. The first is for no surface relaxation and the second is for complete surface relaxation to the ground state.

Mechanisms describing the forces leading to desorption in the MGR model, which may be applicable here, have been discussed by Antoniewicz[47] for adsorbed atoms and Pooley[48] and Hersch[49] for alkali halides. In adapting these models to our system, we assume that initially a surface aluminum atom is further ionized by trapping an exciton or a hole. The atom relaxes towards the surface due to it higher effective charge. If the exciton then decays or an electron is captured, the aluminum now finds itself too close to the surface and experiences a repulsive force and desorbs.

IV. CONCLUSION

The interaction of laser photons with the sapphire (11$\bar{2}$0)-(12×4) surface induces the desorption of highly energetic (~7 eV) aluminum ions. This high kinetic energy indicates the desorption proceeds via an electronic excitation. The stable desorption energy, the preferential desorption of aluminum, and the independence of the translational kinetic energy from laser fluence below the ablation threshold and from laser wavelength (355 and 1064 nm) corroborate this conclusion. The absorption of the photon energy may be aided by the presence of surface electronic states in the band gap as revealed by the 3.6-eV energy-loss feature in the ELS on the (12×4) surface.

The electronic and atomic structures of the surface were affected by the photon absorption as evidenced by changes in the LEED characteristics. With increased laser exposure the crossover energy for the disappearance of charging also increased, showing that the electronic structure is modified. The atomic structural rearrangements were revealed by the disappearance of the 12th-order diffraction beams after sufficient exposure. The laser-induced desorption of aluminum suggests that the fractional-order beams were due to surface aluminum atoms.

The electronic and atomic structure of the equilibrium surface were also investigated. The ELS measurements of the (11$\bar{2}$0)-(12$\times$4) surface were in good agreement with previous measurements of the interband transitions and the bulk plasmon loss. Contrary to a previous report, the equilibrium reconstructed LEED pattern appears to be simply related to the bulk truncation (1$\times$1) geometry, although the unit cell is large.

ACKNOWLEDGMENTS

The authors gratefully acknowledge L. L. Chase and H. W. H. Lee for helpful discussions. This work was supported by the Division of Material Sciences, Office of Basic Energy Sciences, U.S. Department of Energy, at Lawrence Livermore National Laboratory, under Contract No. W-7405-ENG-48.

---

[1] L. L. Chase and L. K. Smith, in *Laser-Induced Damage in Optical Materials*, edited by H. E. Bennet, A. H. Gunther, D. Milam, B. E. Newnham, and M. J. Soileau (National Institute of Standards and Technology, Washington, D.C., 1987), p. 165.

[2] W. L. Smith, Opt. Eng. **17**, 489 (1978).

[3] H. F. Arlinghaus, W. F. Calaway, C. E. Young, M. J. Pellin, D. M. Gruen, and L. L. Chase, J. Appl. Phys. **65**, 281 (1988).

[4] W. J. Siekhaus, J. H. Kinney, D. Milam, and L. L. Chase, Appl. Phys. A **39**, 163 (1986).

[5] R. W. Dreyfus, R. Kelly, and R. E. Walkup, Appl. Phys. Lett. **49**, 1478 (1986).

[6] P. A. Eshbach, J. T. Dickinson, S. C. Langford, L. C. Jensen, L. R. Pederson, and D. R. Baer, in *In-Situ Patterning: Selective Area Deposition and Etching*, edited by A. F. Bernhardt, J. G. Black, and R. Rosenberg, MRS Symposia Proceedings No. 158 (Materials Research Society, Pittsburgh, 1990), p. 463.

[7] J. P. Cowin, D. J. Auerbach, C. Becker, and L. Wharton, Surf. Sci. **78**, 545 (1978).

[8] R. Kelly and R. W. Dreyfus, Surf. Sci. **198**, 263 (1988); Nucl. Instrum. Methods Phys. Res. B **32**, 341 (1988).

[9] J. Reif, H. Fallgren, W. E. Cooke, and E. Matthias, Appl. Phys. Lett. **49**, 770 (1986); J. Reif, H. B. Nielsen, O. Semmler, and E. Matthias, Phys. Scr. **35**, 532 (1987).

[10] C. C. Chang, J. Vac. Sci. Technol. **8**, 500 (1971); J. Appl. Phys. **39**, 5570 (1968); in *The Structure and Chemistry of Solid Surfaces*, edited by G. A. Somorjai (Wiley, New York, 1969), p. 77-1.

[11] T. M. French and G. A. Somorjai, J. Phys. Chem. **74**, 2489 (1970).

[12] J. M. Charig, Appl. Phys. lett. **10**, 139 (1967); J. M. Charig and D. K. Skinner, in *The Structure and Chemistry of Solid Surfaces* (Ref. 10), p. 34-1.

[13] P. S. P. Wei and A. W. Smith, J. Vac. Sci. Technol. **9**, 1209 (1972).

[14] J. Olivier and R. Poirier, Surf. Sci. **105**, 347 (1981).

[15] A. Balzarotti, F. Antonangeli, R. Girlanda, and G. Martino, Phys. Rev. B **29**, 5903 (1984).

[16] W. J. Gignac, R. S. Williams, and S. P. Kowalczyk, Phys. Rev. B **32**, 1237 (1985).

[17] D. R. Haynes, K. R. Helwig, N. J. Tro, and S. M. George, J. Chem. Phys. **93**, 2836 (1990).

[18] S. Ciraci and I. P. Batra, Phys. Rev. B **28**, 982 (1983).

[19] Xia Shangda, Guo Changxin, Lin Libin, and D. E. Ellis, Phys. Rev. B **35**, 7671 (1987).

[20] R. A. Evarestov, A. N. Ermoshkin, and V. A. Lovchikov, Phys. Status Solidi B **99**, 387 (1980).

[21] R. W. Dreyfus, F. A. McDonald, and R. J. von Gutfeld, J. Vac. Sci. Technol. B **5**, 1521 (1987).

[22] A. C. Tam, J. L. Brand, D. C. Cheng, and W. Zapka, Appl. Phys. Lett. **55**, 2045 (1989).

[23] A. L. Hughes and V. Rojansky, Phys. Rev. **34**, 284 (1929).

[24] L. E. Davis, N. C. MacDonald, P. W. Palmberg, G. E. Riach, and R. E. Weber, *Handbook of Auger Spectroscopy* (Physical Electronic Industries, Eden Prairie, MN, 1978).

[25] G. Ertl and J. Küppers, *Low Energy Electrons and Surface Chemistry* (Verlag Chemie, Weinheim, 1974), pp. 150–158.

[26] M. A. Van Hove, W. H. Weinberg, and C.-M. Chan, *Low Energy Electron Diffraction: Experiment, Theory, and Surface Structure Determination* (Springer-Verlag, Berlin, 1986).

[27] A. van Oostrom, Surf. Sci. **89**, 615 (1979).

[28] J. T. Dickinson, S. C. Langford, L. C. Jensen, P. A. Eschbach, L. R. Pederson, and D. R. Baer, J. Appl. Phys. **68**, 1831 (1990).

[29] C. Benndorf, G. Keller, H. Seidel, and F. Thieme, Surf. Sci. **67**, 589 (1977).

[30] M. Bujor, L. A. Larson, and H. Poppa, J. Vac. Sci. Technol. **20**, 392 (1982).

[31] S. Nagai, J. Nucl. Mater. **151**, 275 (1988).

[32] D. W. Fradin and M. Bass, Appl. Phys. Lett. **22**, 206 (1973).

[33] Y. Kumazaki, Y. Nakai, and N. Itoh, Phys. Rev. Lett. **59**, 2883 (1987).

[34] N. Itoh, Nucl. Instrum. Methods Phys. Res. B **27**, 155 (1987).

[35] J. T. Dickinson, L. C. Jensen, and M. R. McKay, J. Vac. Sci. Technol. A **5**, 1162 (1987).

[36] M. A. Schildbach, L. L. Chase, and A. V. Hamza, in Laser-Induced Damage in Optical Materials: 1990, 22nd Annual Boulder Damage Symposium Proceedings, edited by H. E. Bennett, L. L. Chase, A. H. Guenther, B. E. Newnam, and M. J. Soileau [Proc. SPIE **1441**, 287 (1991)].

[37] P. Wurz, J. Sarnthein, W. Husinsky, G. Betz, P. Nordlander, and Y. Wang, Phys. Rev. B **43**, 6729 (1991).

[38] E. D. Johnson, R. F. Garrett, M L. Knotek, and F. Sette, in *Desorption Induced by Electronic Transitions-DIET III*, edited by R. H. Stulen and M. L. Knotek (Springer, Heidelberg, 1988), p. 210.

[39] M. A. Schildbach and A. V. Hamza (unpublished).

[40] M. L. Knotek and P. J. Feibelman, Phys. Rev. Lett. **40**, 964 (1978).

[41] N. Itoh and T. Nakayama, Phys. Rev. Lett. **92A**, 471 (1982).

[42] Y. Nakai, K. Hattori, and N. Itoh, Appl. Phys. Lett. **56**, 1980

(1990).

[43] A. Balzarotti, F. Antonangeli, R. Girlanda, and G. Martino, Solid State Commun. **44**, 275 (1982).

[44] I. A. Brytov and Yu. N. Romashchenko, Fiz. Tverd. Tela Leningrad **20**, 664 (1978) [Sov. Phys. Solid State **20**, 384 (1978)].

[45] D. Menzel and R. Gomer, J. Chem. Phys. **41**, 3311 (1964).

[46] P. A. Redhead, Can. J. Phys. **42**, 886 (1964).

[47] P. R. Antoniewicz, Phys. Rev. B **21**, 3811 (1980).

[48] D. Pooley, Proc. Phys. Soc. London **87**, 245 (1966).

[49] H. N. Hersch, Phys. Rev. **148**, 928 (1966).

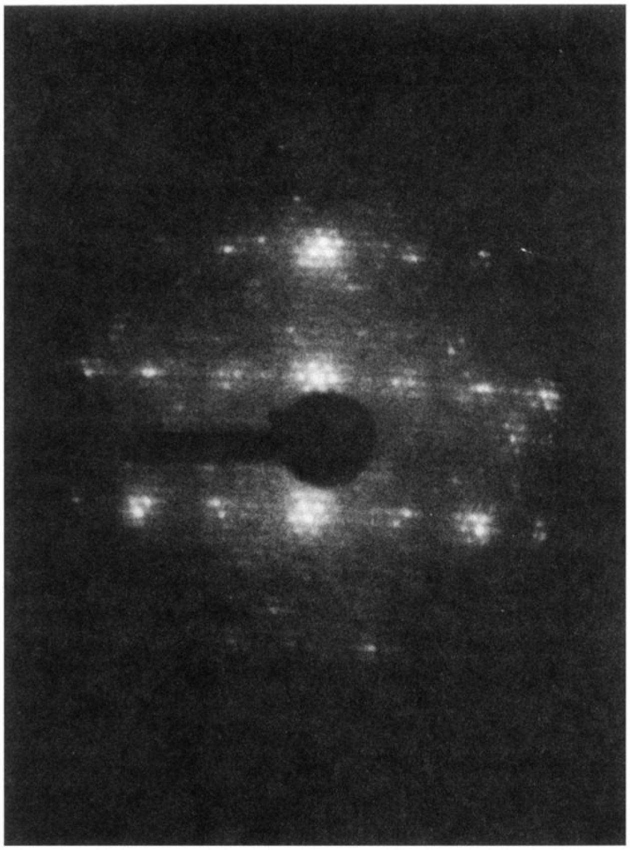

FIG. 2. Low-energy electron diffraction pattern from $Al_2O_3(11\bar{2}0)$ annealed to 1600 K. The incident beam was 5° off normal and had an energy of 143 eV.